Desalination and Water Treatment
www.deswater.com
doi: 10.5004/dwt.2020.26162

202 (2020) 121–132
October

Developing symmetrical traditional double-stage membrane distillation system based on air-gap and water-gap configurations

Mostafa Abd El-Rady Abu-Zeid[a,b], Xiaolong Lu[a,*] , Shaozhe Zhang[a]

[a]*State Key Laboratory of Separation Membranes and Membrane Processes, School of Material Science and Engineering, Institute of Biological and Chemical Engineering, Tiangong University, Tianjin 300387, PR China, Tel. +8613920286131; Fax: +86 22 83955169; emails: 13920286131@163.com (X. Lu), Tel. +201094341146; Fax: +2 064 3320793; emails: mostafa241981@agr.suez.edu.eg/mostafa_2005151@yahoo.com (M.A.E.-R. Abu-Zeid), Tel. +8613072258317; email: 987974282@qq.com (S. Zhang)*
[b]*Department of Agricultural Engineering, Faculty of Agriculture, Suez Canal University, Ismailia 41522, Egypt*

Received 10 December 2019; Accepted 22 May 2020

ABSTRACT

The trade-off between the energy efficiency (i.e., gained output ratio) and permeate flux presented in two-stages of similar air gap membrane distillation (AG-AG)MD arrangement was eliminated by establishing two-stages of new air gap water gap membrane distillation (AG-WG)MD arrangement. The (AG-WG)MD performance was assessed by comparing with (AG-AG)MD under various feed temperatures and flow rates using tap water as feed. Data were subjected to the analyses of the variance and multivariate analysis to test the significant effect of different feed and designs at $p < 0.05$. Results revealed that the feed temperature and flow rate induced highly significant differences ($p < 0.001$***) in permeate flux (P_f), gained output ratio (GOR), waste heat input ($Q_{H,I}$), and specific thermal energy consumption (STEC). Additionally, the (AG-WG)MD could enhance the P_f and GOR, diminish the $Q_{H,I}$ and STEC compared to (AG-AG)MD. It was observed under optimal operating conditions of feed temperature of 50°C, flow rate of 26 L/h, and cooling water temperature of 20°C, the P_f and GOR could be improved by about 31.47% and 14.44%, the STEC, and $Q_{H,I}$ could be reduced by around 33.88% and 12.40%, respectively, from (AG-AG)MD to (AG-WG)MD. Hence, the (AG-WG) MD was found an effective arrangement than the traditional (AG-AG)MD.

Keywords: Permeate flux; Multi-stage membrane distillation; Air-gap membrane distillation; Water-gap membrane distillation; Gained output ratio

1. Introduction

Membrane distillation (MD) is a modern technology used for water desalination by combining with other conventional thermal-driven separation technologies [1]. The membrane distillation thermal driving force is a partial vapor pressure difference generated due to the temperature difference through the hydrophobic and micro-porous membrane [2]. Membrane distillation could be divided depending on the method used for water vapor condensation into four different systems as follows: vacuum membrane distillation (VMD) [3], sweeping gas membrane distillation (SGMD) [4], direct contact membrane distillation (DCMD) [5], and air-gap membrane distillation (AGMD) [6]. Comparing with other separation technologies, membrane distillation achieves very high salt rejection rate at a low operating temperature [7], and pressure [8]. Aforesaid advantages facilitated membrane distillation used in several water treatment applications: seawater desalination [9], water reuse [10], textile [11], olive mill wastewater treatments [12], and shale gas produced water management [13].

* Corresponding author.

Despite the advantages given by membrane distillation technology, however, the problem of low permeate flux and high thermal energy consumption affected profoundly industrialization as mentioned in several previous works. As for example, experimental work proceeded by Shim et al. [14]. The authors pointed out that the DCMD used flat sheet C07 membrane was inefficient process in terms of energy use as compared to reverse osmosis, multistage flash distillation, and multi-effect distillation. The determined gained output ratio (GOR) and thermal energy consumption ranged from 0.44 to 0.70 and from 896 kWh/m^3 to 1,433 kWh/m^3, respectively. The optimal operating conditions for the lowest values of thermal energy consumption, the highest GOR and permeate flux (40.9 L/h m^2) were hot feed temperature of 60°C, cooling water temperature of 20°C, and feed flow rate of 4.5 L/min. As proclaimed by Lewandowicz et al. [15] and Qtaishat et al. [16], the reported values of the energy efficiency (i.e., GOR) were changed between 0.2 and 1.0 for the conventional membrane distillation technology. The minimum gained output ratio values may be caused by the impedance of vapor mass transfer within the dry membrane pores, the conductive heat loss across the membrane, the devastating influences of temperature, and concentration polarization phenomena. Heinzl et al. [17] have mentioned that the energy efficiency of membrane distillation technology could enhance considerably either by heat recovery or design of multi-effect configurations. In this context, Zhang et al. [18] and Li et al. [19] stated that energy efficiency could reach greater than 15 for the multiple-effect distillation system. Lü et al. [20] experimentally assessed the performance of the vacuum multiple-effect membrane distillation (VMEMD) module by comparing it with the conventional VMD module. The experimental outcomes revealed that the VMEMD was an effective module compared to the conventional VMD in terms of fulfilling highest permeate flux (34.8 kg/m^{2}h maximal value) and saving more cooling water consumption which was only 30.8% of conventional VMD at hot feed temperature of 345 K and feed flow rate of 4 L/h. Lee and Kim [21] studied the effect of connecting four-stage VMD in series, parallel, and mixed arrangements on the module flux and water product cost. The authors demonstrated that the mixed arrangement could attain the greatest flux (up to 3.79 m^3/d) and lowest water product cost ($1.16/m^3) at feed temperature of 7°C, feed velocity of 2.4 m/s, and vacuum degree of 4 kPa. In another study, double-stage air gap membrane distillation module was utilized for water desalination [22]. The authors declared that the module fulfilled a maximum cumulative permeate flux and single-stage permeate flux reached up to 128.46 and 65.81 kg/m^{2}h, respectively, at hot feed temperature of 80°C, coolant temperature of 20°C, feed flow rate of 3 L/min, and feed salt concentration of 4.06 g/L. A work by Pangarkar and Deshmukh [23] experimentally investigated the impact of the multi-effect air gap membrane distillation (ME-AGMD) module on the permeate flux. Experimental results showed a maximum permeate flux reached up to 166.38 L/m^{2}h was achieved at feed temperature of 80°C, feed flow rate of 1.5 L/min, coolant temperature of 20°C. In comparison with single-stage AGMD module, the total permeate flux obtained by the ME-AGMD module was higher 3.2–3.6 times, and also thermal efficiency (347.37%) was far greater than a single-stage AGMD (71.78%) at hot inlet feed temperature of 80°C. Khalifa et al. [24] have compared the permeate flux and GOR for the multi-stage (MS-AGMD) and single-stage air gap membrane distillation modules running under two different parallel and series flow stage connections. They elucidated that at high feed temperature of 90°C, the maximum reported values of permeate flux and GOR were about 2.6–3.0 times and 0.45–0.60 for MS-AGMD module under series and parallel connections, respectively. As described by Khalifa and Alawad [25] a comparative study was implemented between three-stage air gap membrane distillation (MS-AGMD) and three-stage water-gap membrane distillation (MS-WGMD) modules. Results showed that the MS-WGMD outperforms significantly MS-AGMD. The permeate flux ratio of water gap to air gap was changed from 2.05 to 2.45 in case of parallel connection and from 2.005 to 2.33 in case of series connection at feed inlet temperatures ranged from 50°C to 90°C, coolant temperature 20°C, and feed salinity of 150 mg/L. Another comparative study by Khalifa [26] demonstrated that the system of the water gap membrane distillation (WGMD) has performed better permeate flux than that of the system of the air gap membrane distillation between 90% and 140% augmentation under inlet feed temperatures from 50°C to 90°C, feed salt concentration of 145 mg/L, and feed flow rate of 1.5 L/min. These results were ascribed to low sensitive to gap thick and less gap temperature which was high in the air gap membrane distillation system. Similarly, Essalhi and Khayet [27] reported increments from 2.2% to 6.5% in the permeate flux of WGMD compared to the permeate flux of air gap membrane distillation at different hot feed temperatures from 35°C to 80°C.

The objective of the current research work is to eliminate the trade-off between the energy efficiency and the permeate flux (i.e., high heat recovery and low permeate flux) existed in two stages of similar air gap membrane distillation (AG-AG)MD arrangement. So, two-stages of new air gap water gap membrane distillation (AG-WG)MD and (WG-AG)MD arrangements were established and evaluated experimentally by comparing with two stages of similar air gap membrane distillation (AG-AG)MD and water gap membrane distillation (WG-WG)MD arrangements. The comparison and assessment were done based on the calculated values of permeate flux (P_f), GOR, specific thermal energy consumption (STEC), and waste heat input ($Q_{H,I}$). The experimental investigations were performed at different hot feed inlet temperatures and feed flow rates using fresh tap water as the feed solution. The reported permeate flux rate is defined as the mass of evaporated molecules in 1 Kg pass through 1 m^2 of membrane pores area and then condense on the cold plate into pure distilled water within 1 h operation time [15,28].

As elaborated in Fig. 1, the key idea of establishment two stages of new (AG-WG)MD and (WG-AG)MD arrangements is making use of the advantage of high internal heat recovery achieved within the WGMD module to increase the temperature of cold feed solution (T_3) before entering air gap membrane distillation module at the permeate side. The cold feed solution condenses the vapor in addition to gains additional heat to become (T_3'). Due to improved mixing taken place in the feed tank, preheated cold feed solution (T_3') rises the temperature of the inlet hot feed solution (T_1).

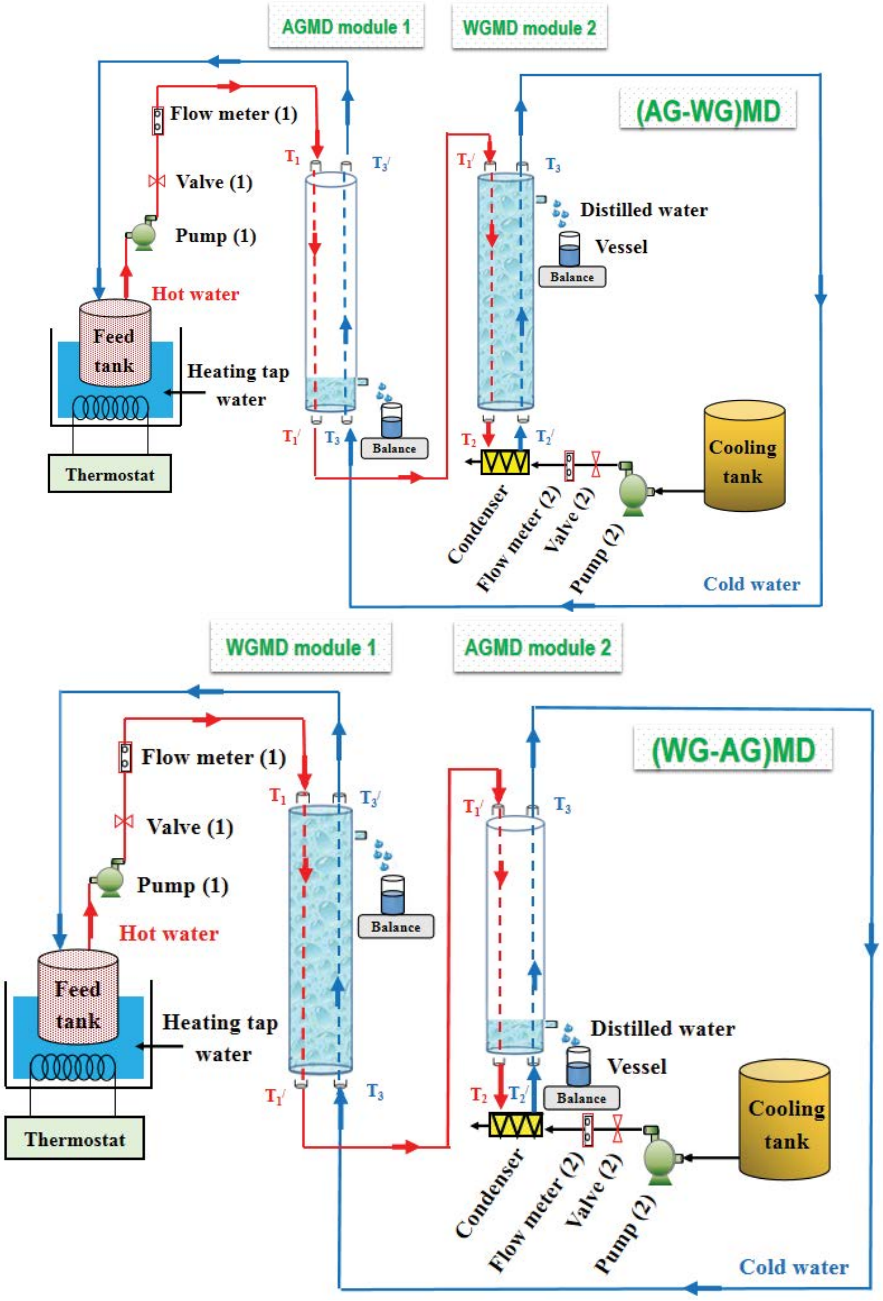

Fig. 1. Schematic diagrams illustrating the two stages of new (AG-WG)MD and (WG-AG)MD arrangements.

Hence, increasing the inlet (T_1) and outlet (T_3') feed solution temperatures increases the temperature difference between the hot and the cold feed at both sides of the membrane ($\Delta T_{cross} = T_1 - T_3'$), then enhanced the permeate flux.

2. Materials and methods

2.1. Experimental equipment set-up and materials

The flow diagrams of two stages of new and similar AGMD and WGMD arrangements are shown in Figs. 1 and 2. Each system has a thermostatic heating bath (Model: CS-501, Tongzhou Branch of Shanghai Jinping Instrument Limited Company, China), digital flow meter (Model: LZB-4, Huanming, Yugao Industrial Automation Instrument Company, Zhejiang, China), circulation pump (Model: MP-55RZ, Shanghai Xinxishan Industrial Limited Company, China), feed tank, cooling tank, valves, external condenser, electronic balance, and vessel. The experiments are carried out using fresh tap water had an electrical conductivity of 515 μS/cm. The width of the gap between the membrane and the cold plate is about 5 mm. Fresh tap water is heated up to the desired inlet feed temperature utilizing a thermostatic heating bath and cold down in an external condenser.

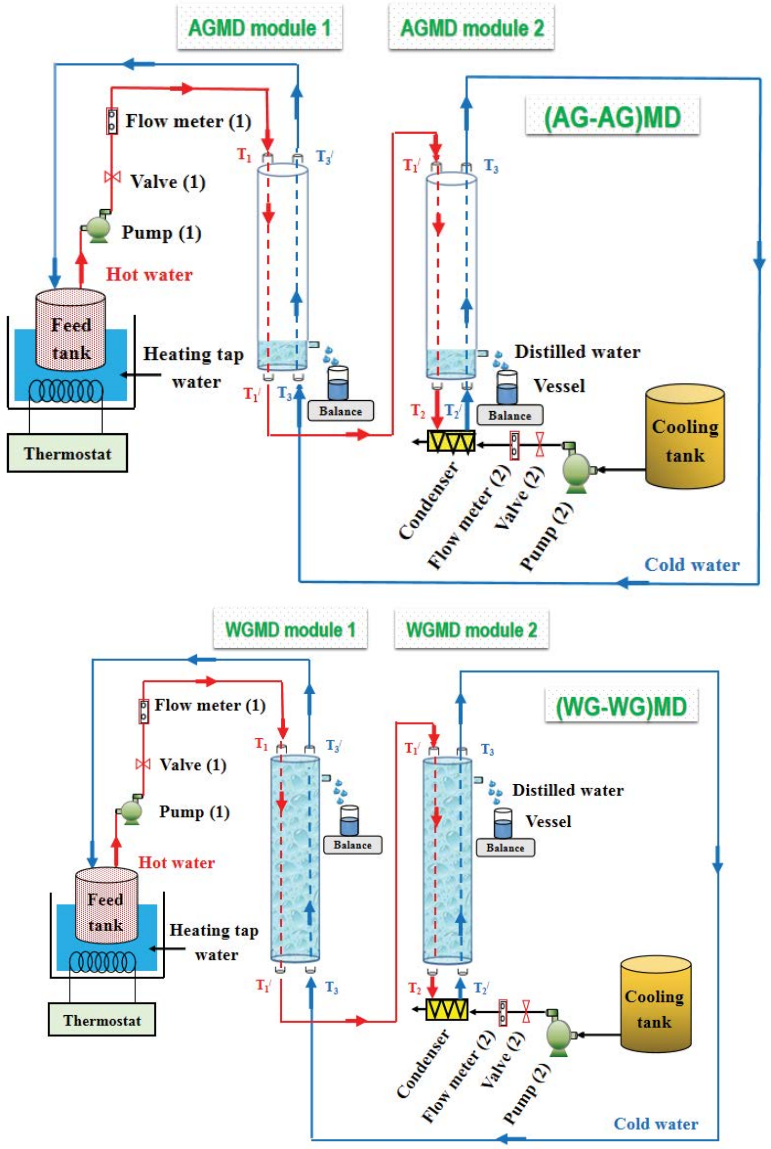

Fig. 2. Schematic diagrams illustrating the two stages of similar (AG-AG)MD and (WG-WG)MD arrangements.

Micro-porous polyvinylidene difluoride (PVDF) hollow fibers membrane and non-porous polypropylene (PP) heat exchange tubes manufactured by our research team are arranged in a counter-current flow. The two modules of the AGMD and WGMD are equipped with internal heat recovery by gathering hollow fibers and heat exchange tubes in a parallel arrangement inside a shell module, filled the distance between fibers and tubes with air (AGMD module) and water (WGMD module). The module shell made of Plexiglas is covered with thermal insulating material to stop any heat loss from the membrane modules to the surrounding environment. The two-stages of new and similar AGMD and WGMD arrangements are connected in series to boost permeate flux, enhance heat recovery, and diminish heating energy consumption. The dimensions of PVDF hollow fibers membrane, PP heat exchange tubes, and membrane modules used in the experiments are shown in Table 1. The detailed specifications of the micro-porous PVDF hollow fibers membrane are tabulated in Table 2.

2.2. Experiment description

In the (AG-WG)MD experiment as presented in Fig. 1, the hot feed solution was pumped from the feed tank into PVDF hollow fibers membrane of the AGMD module 1 and WGMD module 2 top, respectively (referring as a red solid line in the figure) in downward direction where evaporated molecules diffuse across the membrane pores and gap area. After the hot feed solution leaving WGMD module 2 bottom entered the external condenser for a temperature reduce and a thermal driving force. In the opposite direction, the cold feed solution going in PP heat exchange tubes of WGMD module 2 and AGMD module 1 bottom, respectively (referring as a blue solid line in the figure) for internal

Table 1
Dimensions of the PVDF hollow fibers membrane, PP heat exchange tubes, and membrane modules used in the experiments

Hollow fibers type	I.D./O.D. (mm)	Number of hollow fibers membrane and heat exchange tubes	Hollow fibers membrane and heat exchange tubes length (m)	Module length (mm)	*Inner surface area (m^2)
PVDF hollow fibers membrane	0.80/1.10	120	0.59	0.77	0.18
PP heat exchange tubes	0.40/0.50	240	0.59	0.77	0.18

*The inner surface area was determined according to the inner diameter of the PVDF hollow fiber membrane and PP heat exchange tube.

Table 2
Specifications of the micro-porous PVDF hollow fiber membrane

Character	Value
Thickness (μm)	150
Porosity (%)	85
pore size (μm)	0.20
Contact angle (°)	80.5
Bubble point pressure (MPa)	0.11

heat recovery. Finally, the preheated cold feed solution departing AGMD module 1 top returned back to the feed tank to begin a new cycle. It should be mentioned here that the collected pure distilled water returned back to the feed tank for keeping constant both volume and electrical conductivity of the feed solution throughout the experiment.

The performances of the two stages of new and similar AGMD and WGMD arrangements were tested at different hot feed inlet temperatures of 50°C, 60°C, 70°C, and 80°C, and feed flow rates of 14, 18, 22, and 26 L/h (equivalent to cross-flow velocities of 0.065, 0.083, 0.101, and 0.112 m/s, respectively). The hot feed inlet temperature was adjusted by using a temperature controller (XMTD-3001, Easey Commercial Building Hennessy Road Wanchai Hongkong, China). The cooling water temperature was kept stable at 20°C. Temperatures through and between the two membrane modules are continuously monitored using several thermometers installed at the inlets and outlets of the hollow fibers membrane and the heat exchange tubes. The two stages of new and similar AGMD and WGMD arrangements are left running for 60 min before recording different measurements to guarantee no dissolved gases in the feed stream and reach the equilibrium. To make the obtained data more accurate and credibility, each experiment was implemented three times under the same inlet operating conditions and average values are announced. Each experiment test was performed for 1 h. The electrical conductivity of distilled water and feed fresh tap water are measured permanently using a conductivity meter (Model: DDS-11A, Shanghai Leici Xinjing Instrument Company, China) to check for any membrane pore wetting that might have occurred.

2.3. Performance indicators

The performances of two stages of new and similar AGMD and WGMD arrangements were evaluated by measuring the following most important indicators such as permeate flux (P_f), GOR, waste heat input ($Q_{H.I}$), and STEC. Water specific heat (C_p) of 4.1865 KJ/kg°C and water density (ρ_f) of 996.95 kg/m^3 are utilized in the determination. The different measurements such as inlet temperature of the hot feed stream (T_1), outlet temperature of the hot feed stream (T_1'), inlet temperature of the cold feed stream (T_3), and outlet temperature of the cold feed stream (T_3') for the first stage module, outlet temperature of the hot feed stream (T_2), inlet temperature of the cold feed stream (T_2') for the second stage module, and permeate flux (P_f) (Kg/(m^2 h)) are recorded every 10 min and listed in Tables 3 and 4 at different feed hot inlet temperatures (T_f) and feed flow rates (M_f).

2.3.1. Gained output ratio

GOR is determined mathematically by [29,30]:

$$\mathrm{GOR} = \frac{Q_{\mathrm{L.H.,distilled\ water}}}{Q_{\mathrm{H.I.}}} \tag{1}$$

where $Q_{\mathrm{L.H.,\ distilled\ water}}$ and $Q_{\mathrm{H.I}}$ indicated to evaporation latent heat transfer (KJ/h) and waste heat input (KJ/h). They are given by following expressions:

$$Q_{\mathrm{L.H.,distilled\ water}} = P_f \times \Delta H_V \tag{2}$$

$$Q_{\mathrm{H.I.}} = m_f \times C_p \times \Delta T_{\mathrm{cross}} \tag{3}$$

$$Q_{\mathrm{H.I.}} = m_f \times C_p \times \left(T_1 - T_3'\right) \tag{4}$$

where ΔH_V is the latent heat of vaporization (≈2,326 kJ/kg), m_f is the mass feed flow rate (L/h), and C_p is the specific heat of water (KJ/kg°C).

2.3.2. Permeate flux

The permeate flux in kg/(m^2 h) could be calculated as:

$$P_f = \frac{W_f}{S_{\mathrm{inner}} \times t} \tag{5}$$

where W_f is the weight of distilled water within the time of t (Kg), and S_{inner} is the effective evaporation surface area based on the inner diameter of the hollow fiber membranes (m^2).

2.3.3. Specific thermal energy consumption

The STEC (MWh/kg) which indicated to the energy loss of feed bulk flow could be estimated by Eq. (6) [31]:

$$\mathrm{STEC} = \frac{m_f \times \rho_f \times C_p \times \Delta T_{\mathrm{cross}}}{3.6 \times 10^6 \times 10^3 \times P_f} \tag{6}$$

where ρ_f is the feed tap water density (kg/m^3) and the number of (10^3) in the denominator is used for converting the unit from KWh/kg to MWh/kg.

2.3.4. Salt removal factor can determine by

$$\mathrm{SRF} = \frac{\mathrm{SC}_{\mathrm{feed}} - \mathrm{SC}_{\mathrm{distilled\ water}}}{\mathrm{SC}_{\mathrm{feed}}} \tag{7}$$

where $\mathrm{SC}_{\mathrm{feed}}$ is the feed tap water concentration (%) and $\mathrm{SC}_{\mathrm{distilled\ water}}$ is the distilled water concentration (%).

2.4. Statistical analysis

All data were described statistically in terms of means and standard error for means. Data were subjected to the analyses of the variance (ANOVA) and multivariate analysis to test the significant effect of different feed and designs at $p < 0.05$. The effect of studied factors (feeds, designs) and interactions on permeate flux, GOR, energy consumption, and waste heat input were assessed by multivariate analysis at $p < 0.05$. The main effect of a factor were investigated pooling the effects of the other factors/covariates. All statistical analyses were carried out using IBM-SPSS version 23.0 for Mac OS [32,33].

3. Theoretical analysis of heat and mass transfer in two stages of new and similar AGMD and WGMD arrangements

Figs. 3 and 4 show the heat and mass transfer in the two stages of new and similar AGMD and WGMD arrangements utilized in this investigation. In the (AG-AG)MD as for example (Fig. 3), the hot feed solution getting in the AGMD module 1 with mass feed flow rate of $m_{h(\mathrm{AGMD})}$ at the temperature of (T_1) and got out at a temperature of (T_1'). Then, coming in AGMD module 2 with the same mass flow rate of $m_{h(\mathrm{AGMD})}$ at a temperature of (T_1') and stepped out at the temperature of (T_2). Then, the hot feed solution cold down in external condenser to become the temperature of (T_2'). After that, entering AGMD module 2 as a cold feed solution with a mass flow rate of $m_{c(\mathrm{AGMD})}$ at the temperature of (T_2') and went out at the temperature of (T_3). Finally, the preheated cold feed solution going in the AGMD module 1 with the same mass flow rate of $m_{c(\mathrm{AGMD})}$ at the temperature of (T_3) and returned back to the feed tank at a temperature of (T_3').

The overall specific thermal energy consumption ($\mathrm{STEC}_{\mathrm{overall}}$) for 1 Kg of distilled water is calculated mathematically by Eq. (8):

$$\mathrm{STEC}_{\mathrm{overall}} = \frac{m_{h,c} \times \rho_f \times C_p \times \Delta T_{\mathrm{cross}} \left(\frac{\mathrm{AGMD1+AGMD2}}{2}\right)}{3.6 \times 10^6 \times 10^3 \times P_f \left(\mathrm{AGMD1+AGMD2}\right)} \tag{8}$$

The overall gained output ratio ($\mathrm{GOR}_{\mathrm{overall}}$) can be described as:

$$\mathrm{GOR}_{\mathrm{overall}} = \frac{Q_{\mathrm{L.H.,distilled\ water}}}{Q_{\mathrm{H.I.}}} \tag{9}$$

$$Q_{\mathrm{L.H.,\ distilled\ water}} = P_f \left(\mathrm{AGMD1+AGMD2}\right) \times \Delta H_V \tag{10}$$

The overall waste heat input ($Q_{\mathrm{H.I,\ overall}}$) could be determined by:

$$Q_{\mathrm{H.I.,\ overall}} = m_{h,c} \times C_p \times \Delta T_{\mathrm{cross}} \left(\frac{\mathrm{AGMD1+AGMD2}}{2}\right) \tag{11}$$

4. Results and discussion

The calculated P_f, GOR, $Q_{\mathrm{H.I}}$, and STEC values for two stages of similar (AG-AG)MD arrangement are used as a reference for comparison with two stages of new (AG-WG)MD arrangement as declared beneath at various feed temperatures and feed flow rates.

4.1. Comparison between the two stages of new and similar arrangements under different hot feed inlet temperatures (T_f)

Figs. 5a and b show the influence of two stages of new (AG-WG)MD arrangement on the total permeate flux (P_f) and GOR compared to the two stages of similar (AG-AG) MD arrangement. The experimental testing was conducted under various T_f of 50°C, 60°C, 70°C, and 80°C, constant feed flow rate (M_f) of 26 L/h, cooling water temperature of 20°C, and feed electrical conductivity of 515 μS/cm. As presented in Fig. 5a, compared with the (AG-AG)MD, the (AG-WG) MD improved significantly the module permeate flux (P_f) by about 31.47%, 25.45%, 17.81%, and 15.64% at T_f of 50°C, 60°C, 70°C, and 80°C, respectively. The enhanced reported values of permeate flux (P_f) in the case of (AG-WG)MD caused by considerable rise of vapor pressure difference through the membrane as well as a significant reduction in destructive temperature polarization (TP) effect thanks to the integrated effective water gap membrane distillation module. Moreover, the convection heat transfer within the water gap is faster 24.17 times than that of the conduction heat transfer within the air gap (i.e., water and air thermal conductivity are 0.58 and 0.024 W/m K, respectively). This had contributed largely to decrease thermal feed side boundary layer thickness, increase the temperature difference between hot and cold feed at both sides of the membrane ($\Delta T_{\mathrm{cross}} = T_1 - T_3'$), and improve the heat and mass transfer, followed by higher vapor flux unlike (AG-AG)MD. In the case of (AG-AG)MD, the gap filled with air between the membrane and the condensation surface causes a further resistance to vapor mass transfer and temperature decrease in the incoming stage leads to flux decline.

In connection with GOR, increases of about 14.44%, 19.08%, 10.96%, and 9.86% were obtained from (AG-AG)MD to (AG-WG)MD as demonstrated in Fig. 5b. The improved mentioned GOR values in (AG-WG)MD attributed to two reasons. Firstly, low conductive heat loss across the membrane. Secondly, the efficient internal heat recovery achieved

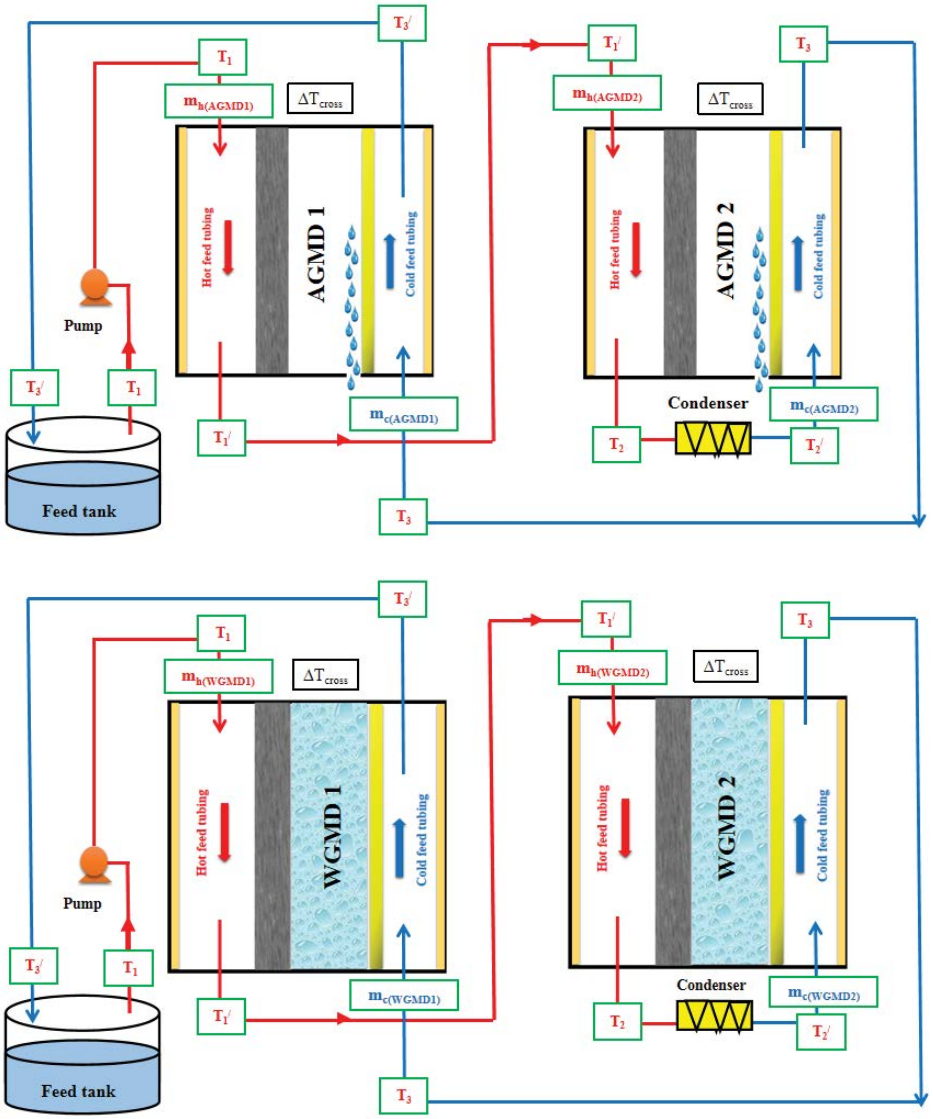

Fig. 3. Heat and mass transfer in the two stages of similar (AG-AG)MD and (WG-WG)MD arrangements.

by the cold feed stream in the heat exchange tubes within the water gap membrane distillation module, resulting in augmented the $\Delta T_{cross} = T_1 - T_3'$ up to 27.00°C, 32.70°C, 38.50°C, and 43.60°C, corresponding to only 23.50°C, 31.00°C, 36.20°C, and 41.50°C in case of (AG-AG)MD (Table 3). On the other side, the minimum GOR values in (AG-AG)MD may be explained as follows: the heat utilized to produce pure distilled water is lesser compared to the heat used for warming the inlet feed solution in addition to lowering air specific heat capacity compared to water leads to insufficient cooling for vapor and hence lower flux (i.e., C_{pw} of air = 993 J/kg°C and C_{pw} of water = 4,200 J/kg°C).

With reference to the STEC and waste heat input ($Q_{H.I}$), it was observed from the experimental outcomes that the STEC was declined by about 33.88%, 33.16%, 23.46%, and 21.21% and also the $Q_{H.I}$ by around 12.40%, 15.69%, 9.43%, and 9.15% from (AG-AG)MD to (AG-WG)MD, as illustrated in Figs. 5c and d. The efficient internal heat recovery achieved within (AG-WG)MD and higher GOR explained low STEC and $Q_{H.I}$ values.

According to the multivariate statistical analysis presented in Figs. 5a–d, the main effect of hot inlet feed temperature, design, and interaction between hot inlet feed temperature and design were assessed by multivariate analysis at $p < 0.05$ level. The effects of previous factors were assessed by also pooling the effects of the other factors/covariates. According to multivariate analysis, feed temperature-induced highly significant differences ($p < 0.001$***) in permeate flux, GOR, energy consumption, and waste heat input.

4.2. Comparison between the two stages of new and similar arrangements under different feed flow rates

Figs. 6a–d display the change of the permeate flux, GOR, STEC, and waste heat input for two stages of new and similar arrangements. Experiments were performed at different

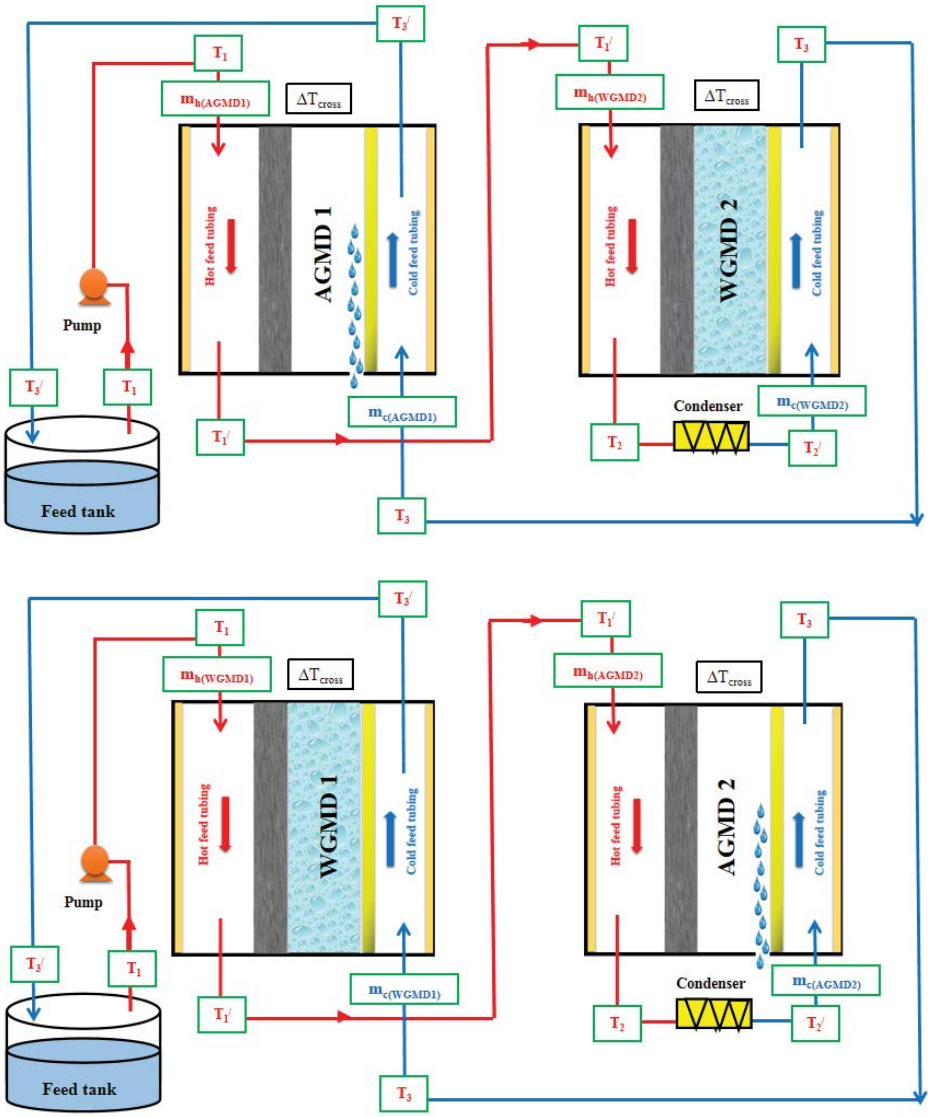

Fig. 4. Heat and mass transfer in the two stages of new (AG-WG)MD and (WG-AG)MD arrangements.

feed flow rates (M_f) of 14, 18, 22, and 26 L/h, and stable hot feed temperature of 80°C, cooling water temperature of 20°C, and feed electrical conductivity of 515 μS/cm. In comparison with (AG-AG)MD, Fig. 6a declared that the (AG-WG)MD enhanced the permeate flux by about 23.64%, 16.46%, 14.62%, and 15.64% at M_f of 14, 18, 22, and 26 L/h, respectively. Two reasons explicated the permeate flux enhancement. Firstly, less temperature polarization (TP) impact (i.e., reduce thermal boundary layer thickness). Secondly, weak resistance to the evaporated molecules which condenses directly at the membrane/water gap interface.

As for GOR, increments of 17.65%, 11.46%, 10.00%, and 9.86% were fulfilled from (AG-AG)MD to (AG-WG)MD as seen in Fig. 6b. The enhancement of GOR associated with the following factors. Firstly, a significant change in mass and heat transfer by virtue of water filled the gap region. Secondly, increase the amount of heat absorbed by the cold feed solution and decrease the conductive heat loss across the membrane. Thirdly, raise the ΔT_{cross} up to 38.70°C, 39.90°C, 41.80°C, and 43.60°C, corresponding to only 36.80°C, 38.20°C, 40.10°C, and 41.50°C in the case of (AG-AG)MD (Table 4). These results could be interpreted by an effective water gap membrane distillation module in reducing thermal boundary layer thickness at the membrane surface. Also, getting high GOR contributed to saving more thermal energy consumption and waste heat input into the module. As can be shown in Figs. 6c and d, the (AG-WG)MD decreased largely the STEC values by about 30.89%, 23.24%, 20.36%, and 21.21% and similarly $Q_{H.I}$ by 15.31%, 9.92%, 9.59%, and 9.15%. It is worth mentioning that the hollow fibers PVDF membrane employed in this investigation demonstrated a salt rejection rate above 99% for both new and similar arrangements.

The multivariate analysis for the effect of designs, feed flow rates were presented in Figs. 6a–d. According to multivariate analysis, the feed flow rate induced highly significant

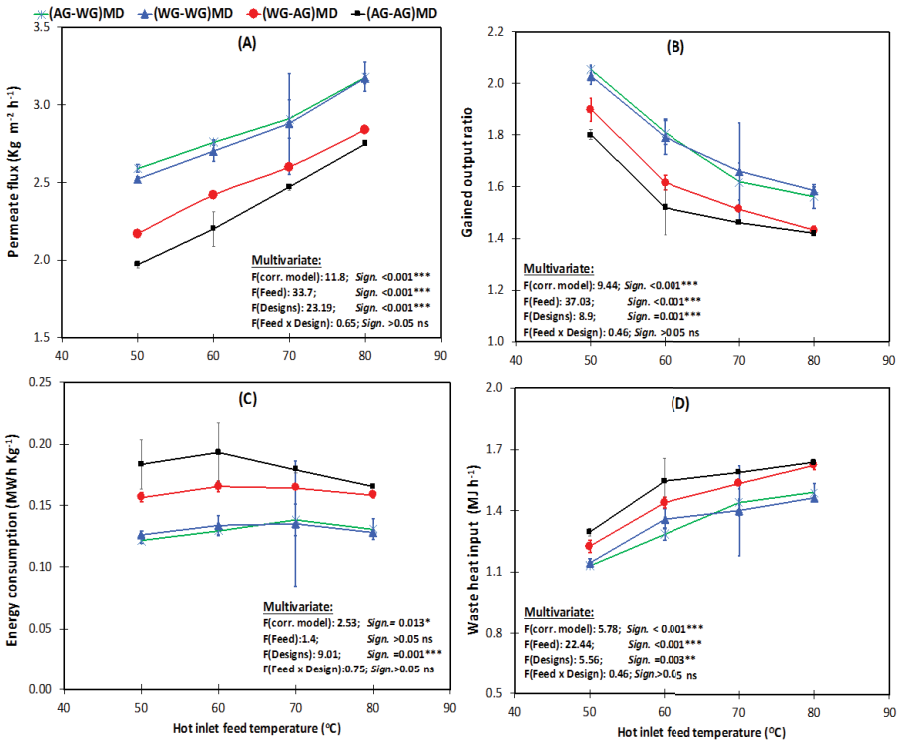

Fig. 5. (a) Permeate flux, (b) gained output ratio, (c) specific thermal energy consumption, and (d) waste heat input as a function of feed inlet temperature for two stages of new and similar AGMD and WGMD arrangements.

Table 3
Different temperatures of T_1, T_1',T_2, T_2', T_3, and T_3' at various hot feed inlet temperature (T_f)

T_f (°C)	T_1	T_1'	T_2	T_2'	T_3	T_3'
(AG-WG)MD						
50	54.70	40.60	31.80	19.50	22.70	27.70
60	61.50	44.90	33.90	19.00	24.30	28.80
70	69.80	50.60	36.60	19.00	24.70	31.30
80	79.90	56.70	40.10	18.70	30.60	36.30
(WG-WG)MD						
50	53.80	40.50	31.10	19.80	22.10	27.20
60	60.70	45.00	33.30	19.60	23.80	28.40
70	67.90	49.30	36.00	19.20	24.20	30.80
80	78.60	56.10	39.60	18.90	29.90	35.80
(WG-AG)MD						
50	51.40	38.90	30.80	19.80	20.90	26.90
60	59.80	44.60	32.80	19.50	21.00	27.70
70	67.00	48.90	35.50	19.30	22.00	30.20
80	77.70	55.30	39.00	19.30	27.20	35.20
(AG-AG)MD						
50	49.20	38.20	29.80	19.70	18.10	25.70
60	58.30	43.50	31.80	19.70	17.50	27.30
70	65.50	49.20	34.90	19.50	17.50	29.30
80	76.20	53.80	38.50	19.60	17.70	34.70

Table 4
Different temperatures of T_1, T_1', T_2, T_2', T_3 and T_3' at various feed flow rate (M_f)

M_f (L/h)	T_1	T_1'	T_2	T_2'	T_3	T_3'
(AG-WG)MD						
14	81.80	53.00	31.30	19.40	34.40	43.10
18	81.30	54.70	35.30	19.30	33.10	41.40
22	80.70	55.70	38.70	19.00	32.00	38.90
26	79.90	56.70	40.10	18.70	30.60	36.30
(WG-WG)MD						
14	80.10	52.70	29.80	19.40	33.80	42.20
18	80.20	54.00	33.20	19.40	32.40	40.10
22	79.30	55.20	37.00	19.20	31.50	37.50
26	78.60	56.10	39.60	18.90	29.90	35.80
(WG-AG)MD						
14	78.20	51.40	27.70	19.80	31.60	40.80
18	78.00	53.20	31.80	19.60	30.00	38.40
22	78.00	54.30	36.70	19.30	28.80	37.00
26	77.70	55.30	39.00	19.30	27.20	35.20
(AG-AG)MD						
14	77.20	51.20	25.70	19.80	29.80	40.40
18	75.00	51.70	28.80	19.70	28.10	36.80
22	75.30	52.60	35.90	19.50	26.00	35.20
26	76.20	53.80	38.50	19.60	17.70	34.70

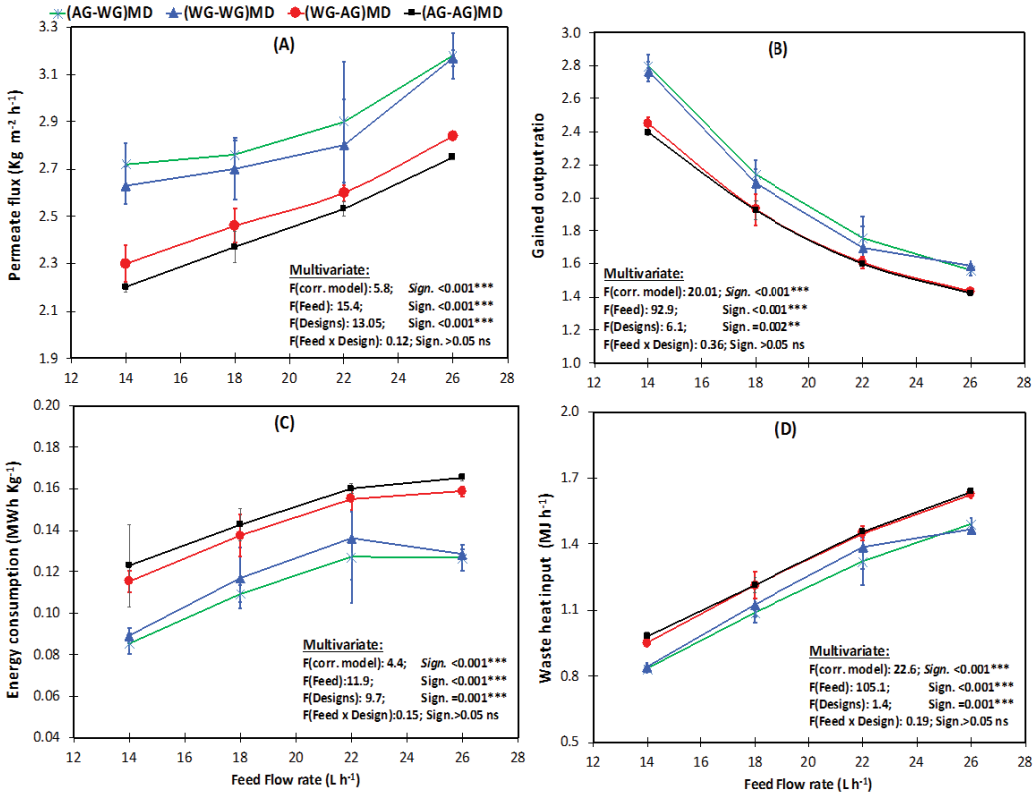

Fig. 6. (a) Permeate flux, (b) gained output ratio, (c) specific thermal energy consumption, and (d) waste heat input as a function of feed flow rate for two stages of new and similar AGMD and WGMD arrangements.

Table 5
Comparisons between the GOR of the two-stages of new (AG-WG)MD system in this study and available values formerly mentioned in the literature data

Reference	Membrane		Operating conditions	Multistage MD system in series	GOR
	Type	Specifications			
Current study	PVDF Hollow fiber	Thickness = 150 μm, porosity = 85%, pore size = 0.20 μm, contact angle = 80.5°, bubble point pressure = 0.11 MPa	T_f = 80°C, T_c = 20°C, M_f = 14 L/h, C_f = 515 μS/cm-Tap water	(AG-WG)MD (2 stage)	2.8
[34]	PTFE hollow fiber	Thickness = 40 mm, porosity = 50–60%, pore size = 0.20–0.25 μm, bubble point pressure = 0.10–0.12 MPa	T_f = 60°C, T_c = 20°C, M_f = 1 L/min, C_f = 253 ppm-tap water	AGMD (2 stage)	1.23
				V-AGMD (2 stage)	1.28
[24]	PTFE Flat plate	Porosity = 80%, pore size = 0.45 μm, effective permeation area of membrane in each module = 0.0074 m²	T_f = 90°C, T_c = 20°C, M_f = 2.3 L/min, C_f = 150 mg/L-tap water	MS-AGMD (3 stage)	0.45
[35]	PTFE flat plate	Thickness = 175 μm, porosity = 70%, pore size = 0.45 μm, membrane area of AGMD module = 80 cm²	T_f = 80°C, M_f = 0.5 L/min, C_f = 4,630 mg/L- (conductivity = 14,350 μs/cm)-synthetic wastewater	ME-AGMD (4 stage)	1.19
[36]	PTFE flat plate	Thickness of PTFE layer = 20 μm, pore size = 0.20 μm, membrane area of one module = 0.159 m²	T_f = 70°C, M_f = 40 L/h, C_f = 300 μs/cm conductivity)-tap water	Memsys V-MEMD module (4 stage)	2.2

differences ($p < 0.001$***) in permeate flux, GOR, energy consumption, and waste heat input.

5. GOR comparison with literature

GOR comparisons between the two-stages of new (AG-WG)MD tested in the current experimental work and other two-stages of similar (AG-AG)MD mentioned in the literature are provided in Table 5. Under the optimal operating conditions (i.e., hot feed inlet temperature and feed flow rate), our two-stages of new (AG-WG)MD achieved the greatest GOR values even when comparing with vacuum-assisted AGMD module [34]. This comparison confirmed the effective impact of connecting WGMD with AGMD module in series on improving module GOR.

6. Conclusions

The present research work established two-stages of new (AG-WG)MD to eradicate the trade-off between the energy efficiency and the permeate flux presented in the two-stages of similar (AG-AG)MD. The (AG-WG)MD performance was evaluated by comparing with the (AG-AG)MD under different feed inlet temperatures and feed flow rates utilizing fresh tap water as the feed solution. Experimental results showed that the (AG-WG)MD achieved the highest permeate flux (P_f) and GOR, the lowest waste heat input ($Q_{H.I}$), and STEC in comparison to the (AG-AG)MD. Under optimal operating conditions of feed inlet temperature of 50°C, feed flow rate of 26 L/h, cooling water temperature of 20°C, and feed electrical conductivity of 515 μS/cm, the P_f and GOR improved by 31.47% and 14.44%, STEC, and $Q_{H.I}$ diminished by 33.88% and 12.40% from (AG-AG)MD to (AG-WG)MD. According to multivariate analysis, both hot inlet feed temperature and feed flow rate induced highly significant differences ($p < 0.001$***) in permeate flux, GOR, energy consumption, and waste heat input. The (AG-WG)MD proved to be more attractive than (AG-AG)MD for an efficient multistage system.

Symbols

AGMD	—	Air-gap membrane distillation
(AG-AG)MD	—	Two stages of similar air-gap membrane distillation arrangement
(AG-WG)MD	—	Two stages of new air-gap-water-gap membrane distillation arrangement
C_P	—	Specific heat of water, KJ/kg°C
GOR	—	Gained output ratio, dimensionless
P_f	—	Permeate flux, kg/(m^2 h)
$Q_{L.H., distilled water}$	—	Evaporation latent heat transfer, KJ/h
$Q_{H.I}$	—	waste heat input, KJ/h
S_{inner}	—	Effective evaporation surface area based on inner diameter of the hollow fiber membranes, m^2
STEC	—	Specific thermal energy consumption, MWh/kg
SRF	—	Salt removal factor, %
SC_{feed}	—	Feed tap water concentration, %
$SC_{distilled\ water}$	—	Distilled water concentration, %
t	—	Time, minute
T_1	—	Inlet temperature of the hot feed stream, °C (first stage)
$T_1^/$	—	Outlet temperature of the hot feed stream, °C (first stage)
T_2	—	Outlet temperature of the hot feed stream, °C (second stage)
$T_2^/$	—	Inlet temperature of the cold feed stream, °C (second stage)
T_3	—	Inlet temperature of the cold feed stream, °C (first stage)
$T_3^/$	—	Outlet temperature of the cold feed stream, °C (first stage)
T_f	—	Hot inlet feed temperatures, °C
M_f	—	Feed flow rate, L/h
W_f	—	Weight of distilled water, Kg
WGMD	—	Water-gap membrane distillation
(WG-WG)MD	—	Two stages of similar water-gap membrane distillation arrangement
(WG-AG)MD	—	Two stages of new water-gap-air-gap membrane distillation arrangement
ΔT_{cross}	—	Temperature difference between hot and cold feed at both sides of the membrane, °C
ΔH_V	—	Latent heat of vaporization, ≈2,326 kJ/kg
ρ_f	—	Density of water, Kg/m^3

Acknowledgments

Supported by the Program for Innovative Research Team in University of Tianjin (No. TD13-5044). Supported by the Program for Changjiang Scholars and Innovative Research Team in University (PCSIRT) of Ministry of Education of China (Grand no. IRT17_R80). National Center for International Joint Research on Separation Membranes, Tianjin Polytechnic University, Tianjin 300387, China.

References

[1] A.A. Al-Ghamdi, Recycling of reverse osmosis (RO) reject streams in brackish water desalination plants using fixed bed column softener, Energy Procedia, 107 (2017) 205–211.
[2] A. Ruiz-Aguirre, J.A. Andrés-Mañas, J.M. Fernández-Sevilla, G. Zaragoza, Modeling and optimization of a commercial permeate gap spiral wound membrane distillation module for seawater desalination, Desalination, 419 (2017) 160–168.
[3] A. Karanasiou, M. Kostoglou, A. Karabelas, An experimental and theoretical study on separations by vacuum membrane distillation employing hollow-fiber modules, Water, 10 (2018), doi: 10.3390/w10070947.
[4] V. Perfilov, V. Fila, J.S. Marcano, A general predictive model for sweeping gas membrane distillation, Desalination, 443 (2018) 285–306.
[5] A. Ali, J.-H. Tsai, K.-L. Tung, E. Drioli, F. Macedonio, Designing and optimization of continuous direct contact membrane distillation process, Desalination, 426 (2018) 97–107.
[6] Z. Liu, S. Zhang, X. Lu, Porous heat exchange tube with ultra-thin dense skin layer via NIPS for AGMD process, J. Membr. Sci., 597 (2020), doi: 10.1016/j.memsci.2019.117782.
[7] M. Khayet, T. Matsuura, Membrane Distillation, Elsevier, Amsterdam, 2011, pp. 1–16.
[8] M.R. Qtaishat, F. Banat, Desalination by solar powered membrane distillation systems, Desalination, 308 (2013) 186–197.
[9] Q.S. Lee, S. Lee, Fouling analysis and control in a DCMD process for SWRO brine, Desalination, 367 (2015) 21–27.

[10] T. Husnain, Y. Liu, R. Riffat, B. Mi, Integration of forward osmosis and membrane distillation for sustainable wastewater reuse, Sep. Purif. Technol., 156 (2015) 424–431.
[11] N. Dow, J.V. García, L. Niadoo, N. Milne, J. Zhang, S. Gray, M. Duke, Demonstration of membrane distillation on textile waste water: assessment of long term performance, membrane cleaning and waste heat integration, Environ. Sci. Water Res. Technol., 3 (2017) 433–449.
[12] A. El-Abbassi, A. Hafidi, M. Khayet, M.C. García-Payo, Integrated direct contact membrane distillation for olive mill wastewater treatment, Desalination, 323 (2013) 31–38.
[13] J. Kim, H. Kwon, S. Lee, S. Lee, S. Hong, Membrane distillation (MD) integrated with crystallization (MDC) for shale gas produced water (SGPW) treatment, Desalination, 403 (2017) 172–178.
[14] W.G. Shim, K. He, S. Gray, I.S. Moon, Solar energy assisted direct contact membrane distillation (DCMD) process for seawater desalination, Sep. Purif. Technol., 143 (2015) 94–104.
[15] G. Lewandowicz, W. Białas, B. Marczewski, D. Szymanowska, Application of membrane distillation for ethanol recovery during fuel ethanol production, J. Membr. Sci., 375 (2011) 212–219.
[16] M. Qtaishat, T. Matsuura, B. Kruczek, M. Khayet, Heat and mass transfer analysis in direct contact membrane distillation, Desalination, 219 (2008) 272–292.
[17] W. Heinzl, S. Büttner, G. Lange, Industrialized modules for MED desalination with polymer surfaces, Desal. Water Treat., 42 (2012) 177–180.
[18] Y.G. Zhang, Y.L. Peng, S.L. Ji, Z.H. Li, P. Chen, Review of thermal efficiency and heat recycling in membrane distillation processes, Desalination, 367 (2015) 223–239.
[19] X.J. Li, Y.J. Qin, R.L. Liu, Y.P. Zhang, K. Yao, Study on concentration of aqueous sulfuric acid solution by multiple-effect membrane distillation, Desalination, 307 (2012) 34–41.
[20] S.L. Lü, Q.J. Gao, X.L. Lü, Device and process study on vacuum multiple-effect membrane distillation, J. Adv. Mater. Res., 573–574 (2012) 120–125.
[21] J.G. Lee, W.S. Kim, Numerical study on multi-stage vacuum membrane distillation with economic evaluation, Desalination, 339 (2014) 54–67.
[22] D.U. Lawal, A.E. Khalifa, Experimental investigation of an air gap membrane distillation unit with double-sided cooling channel, Desal. Water Treat., 57 (2015) 1–15.
[23] B.L. Pangarkar, S.K. Deshmukh, Theoretical and experimental analysis of multi-effect air gap membrane distillation process (ME-AGMD), J. Environ. Chem. Eng., 3 (2015) 2127–2135.
[24] A.E. Khalifa, S.M. Alawad, M.A. Antar, Parallel and series multistage air gap membrane distillation, Desalination, 417 (2017) 69–76.
[25] A.E. Khalifa, S.M. Alawad, Air gap and water gap multistage membrane distillation for water desalination, Desalination, 437 (2018) 175–183.
[26] A.E. Khalifa, Water and air gap membrane distillation for water desalination – an experimental comparative study, Sep. Purif. Technol., 141 (2015) 276–284.
[27] M. Essalhi, M. Khayet, Application of a porous composite hydrophobic/hydrophilic membrane in desalination by air gap and liquid gap membrane distillation: a comparative study, Sep. Purif. Technol., 133 (2014) 176–186.
[28] R. Thiruvenkatachari, M. Manickam, T.O. Kwon, I.S. Moon, J.W. Kim, Separation of water and nitric acid with porous hydrophobic membrane by air gap membrane distillation (AGMD), Sep. Sci. Technol., 41 (2006) 3187–3199.
[29] K. Yao, Y. Qin, Y. Yuan, L. Liu, F. He, Y. Wu, A continuous-effect membrane distillation process based on hollow fiber AGMD module with internal latent-heat recovery, AlChE J., 59 (2013) 1278–1297.
[30] H.X. Geng, Q.F. He, H.Y. Wu, P.L. Li, C.Y. Zhang, H.Y. Chang, Experimental study of hollow fiber AGMD modules with energy recovery for high saline water desalination, Desalination, 344 (2014) 55–63.
[31] H.C. Duong, P. Cooper, B. Nelemans, T.Y. Cath, L.D. Nghiem, Evaluating energy consumption of air gap membrane distillation for seawater desalination at pilot scale level, Sep. Purif. Technol., 166 (2016) 55–62.
[32] R.G. O'Brien, M.K. Kaiser, MANOVA method for analyzing repeated measures designs: an extensive primer, Psychol. Bull., 97 (1985) 316–333.
[33] J. MacInnes, An Introduction to Secondary Data Analysis with IBM SPSS Statistics, Sage Publications Ltd., Los Angeles, 2017.
[34] M.A.E.R. Abu-Zeid, L. Zhang, W.Y. Jin, T. Feng, Y. Wu, H.L. Chen, L. Hou, Improving the performance of the air gap membrane distillation process by using a supplementary vacuum pump, Desalination, 384 (2016) 31–42.
[35] B.L. Pangarkar, S.K. Deshmukh, P.V. Thorat, Energy efficiency analysis of multi-effect membrane distillation (MEMD) water treatment, Int. J. Chem. Tech. Res., 9 (2016) 279–289.
[36] E.S. Mohamed, P. Boutikos, E. Mathioulakis, V. Belessiotis, Experimental evaluation of the performance and energy efficiency of a vacuum multi-effect membrane distillation system, Desalination, 408 (2017) 70–80.